Materials Today: Proceedings 59 (2022) 1846–1851

Contents lists available at ScienceDirect

Materials Today: Proceedings

journal homepage: www.elsevier.com/locate/matpr

Effect of beam oscillation on the fluid flow during laser welding

Anand Mohan *, Dariusz Ceglarek, Michael Auinger

Warwick Manufacturing Group (WMG), University of Warwick, Coventry CV4 7AL, UK

ARTICLE INFO

Article history:
Available online 29 April 2022

Keywords:
Numerical simulation
Temperature profile
Fluid flow
Beam oscillation
Laser welding

ABSTRACT

In the present study, a finite element based numerical model is developed to evaluate heat transfer and fluid flow during the laser welding process with a moving heat source. The developed model solves the fully coupled equations of incompressible fluid flow and heat transfer. In this study, laser beam welding involving non-oscillating to oscillating beam is compared with both conditions under similar heat input per unit length i.e., same power and welding speed. Dimensionless coefficients for mass and heat transport were used to analyse the effects of Marangoni flow and thermal buoyancy. Varying combinations of radius and frequency of oscillations are studied at a constant circumferential velocity.

1. Introduction

Joining Aluminium alloys in the automotive and aerospace industries is the main research focus of welding and joining for fabricating lightweight structures. Laser welding poses a great potential to be used to join these materials with high accuracy and efficiency due to several advantages like high energy density, localised heat input, narrow heat-affected zone (HAZ) and fusion zone (FZ) [1]. Laser welding of Aluminium is a challenging task due to the high reflectivity of the laser beam, high thermal conductivity, and evaporation of alloying elements. The high cooling rate and thermal gradient lead to the formation of hardening structures and residual stresses, which in turn lead to the formation of microcracks and an increase in brittleness of weldments during laser welding [2].

Earlier studies in electron beam welding have demonstrated that beam oscillation has the potential to improve solidification characteristics and weld pool morphology [3,4]. This progresses helped with the development of laser welding with beam oscillation. Beam oscillation leads to wider weld zones, more uniform weld shapes, higher penetration and lowers the cooling rate, which is very high for laser welding. It leads to stabilization of processes [5], lower spatter formation [6], more homogenous weld cross-section [7], improves mechanical strength [8] and reduces porosity formation [9]. It was reported that beam oscillation provides more flexibility to modify the temperature and flow field during the laser welding and produces the churning action in the molten metal pool which increases the mixing and decreases the segregation of alloying elements [8,10]. Beam oscillation leads to the formation of a wider melt pool which can improve the fit-up gap tolerance of the laser welding when joining imperfect edges such as in tailored blanks [11].

The shape and dimension of the weld pool, cooling rate and thermal gradient, are important parameters that determine microstructural attributes such as weld strength and grain morphology during laser welding. Therefore, the history of temperature distribution and fluid flow has an important causal relationship with the solidification behaviour and weld shape [12,13]. These are critical metallurgical factors as they govern the cooling rate, thermal gradient and solidification rate that affect the weld microstructure and mechanical properties. Busuttil *et al.* welded Aluminum 6xxx using beam oscillation and concluded that beam oscillation decreases the thermal gradient within the molten pool [14]. Wang *et al.* concluded that beam oscillation improves the weld ductility using a circular oscillation pattern [10]. Wang *et al.* found that the beam oscillation increases weld width and improves the tensile strength of 5A06 Aluminum alloys [8].

All the studies have shown that beam oscillation improves the weld quality and stabilizes the welding process, leading to a better surface finish and less spatter formation. However, most studies related to Aluminum alloys focus on the process stability and are carried out at a lower frequencies. While some research has reported on the effect of beam oscillation on the thermal cycle [15], however, to date, no study has investigated the effect of beam oscillation on the thermal cycle and flow behaviour for a constant heat input per unit length. The influence of beam oscillation, however, is important and can be understood when the heat input per

* Corresponding author.
E-mail address: a.mohan.2@warwick.ac.uk (A. Mohan).

https://doi.org/10.1016/j.matpr.2022.04.435

unit length is kept constant for each oscillation frequency. A change in heat input would alter the thermal as well as flow behaviour, which makes it difficult to understand the effect of beam oscillation in its entirety. In the present work, a three-dimensional heat transfer and fluid flow model is developed for Al-5083 to investigate temperature distributions and fluid flow behaviour during laser butt welding with and without beam oscillation. This study will also investigate the effect of beam oscillation on the thermal and fluid flow regimes. The effects of natural convection, gravity, surface tension and forced convection due to the beam oscillation are considered. The developed model is validated using experimental results, reported in the literature [13]. Because experimental measurements of the flow during laser welding are difficult to obtain due to the short time-spans, this study focuses on a numerical approach. The reliability of the developed model is analysed, based on the dimensionless numbers for flow and heat transport. These numbers also provide the information to analyse the effect of driving forces such as surface tension and buoyancy force during laser welding.

2. Numerical modelling

A three-dimensional heat transfer and fluid flow model has been developed using a volumetric Gaussian heat source. A three-dimensional Cartesian coordinate system is used where the positive *x*-axis direction is the welding direction, the *y*-axis is the weld cross-section direction and the *z*-axis is the weld penetration direction. The motion of the heat source during beam oscillation is composed of two parts in the *x*-*y* plane, one is a circular motion and the other is a linear forward motion in the welding direction. The overall trajectory of the heat source is typically a spiral. The following assumptions were made during the development of the numerical model: (a) the fluid is considered incompressible and the flow is laminar (as the typical range of Reynolds Number is 300–400 in this study); (b) to decrease the computational time, the model was simplified and keyhole dynamics are not considered but instead a volumetric heat source model is used to replicate the keyhole which is a common practice as described in [16]; (c) no vapour and plasma flow is simulated in the model; (d) the effect of shielding gas on the heat transfer and fluid flow is ignored.

2.1. Governing equations for fluid flow and boundary conditions

A three-dimensional model based on the finite element method (FEM), was developed using COMSOL Multiphysics. To determine velocity fields, a transient fluid flow model was developed based on the solution of the equations of conservation of mass and momentum as given in Eq. (1) [13]. $\nabla.u = 0$ is the mass conservation equation for an incompressible flow.

$$\rho\frac{\partial(u)}{\partial t} = -\rho(u\cdot\nabla)u - \nabla P + \eta\left(\nabla^2 u\right) + F \tag{1}$$

where u is the velocity vector, ρ is the fluid density P is the static pressure, η is the dynamic viscosity of the fluid and F is the force term. The first term in Eq. (2) is according to the Carman-Kozeny equation for flow through a porous media [12] representing the frictional dissipation which ensures a smooth transition of velocity from zero to a large value in the mushy zone. The second term on the right-hand side of Eq. (2) accounts for the natural convection.

$$F = C\left(-\frac{(1-f_l)^2}{f_l^3+B}\right)u + \rho g\beta(T - T_{melting}) \tag{2}$$

where B is a merely computational constant, very small positive number to avoid division by zero is set at 0.001 and C is a mushy zone constant related to the morphology of the porous media which is a large number (a value of 1.6×10^4 was used in the present study) to force velocity of the solid zone to be zero and represents mushy zone morphology, β is the coefficient of volume expansion, g is the acceleration due to gravity, $T_{melting}$ is the melting temperature which is average of solidus and liquidus temperature and f_l is the fraction of liquid which is defined in Eq. (3), where, T_{liq} and T_{sol} are liquidus and solidus temperature of the materials respectively.

$$f_l = \begin{cases} 1 & T > T_{liq} \\ \frac{T-T_{sol}}{T_{liq}-T_{sol}} & T_{sol} \le T \le T_{liq} \\ 0 & T < T_{sol} \end{cases} \tag{3}$$

Flow condition for the free liquid surface due to the surface tension gradient is given by Eq. (4) which states that the temperature gradient is proportional to shear stress on the surface and $\partial\gamma/\partial T$ is the temperature coefficient of surface tension.

$$-\eta\frac{\partial u_x}{\partial z} = \frac{\partial\gamma}{\partial T}\frac{\partial T}{\partial x}; -\eta\frac{\partial u_y}{\partial z} = \frac{\partial\gamma}{\partial T}\frac{\partial T}{\partial y}; u_z = 0 \tag{4}$$

2.2. Governing equations for heat transfer and boundary conditions

To determine temperature fields, a transient heat transfer model was developed based on the solution of the equation of conservation of energy formulated as [13].

$$\rho C_P\frac{\partial T}{\partial t} + \rho C_P u\cdot\nabla T = \nabla\cdot(\lambda\nabla T) + Q_{laser} + Q_{vap} \tag{5}$$

where C_P is the specific heat capacity of the material, T is the temperature of the workpiece, t is the time, λ is the thermal conductivity of the material, Q_{laser} is the energy input of the laser heat source and Q_{vap} is the energy loss by evaporation. The phase changes are considered to include temperature change due to latent heat by using the apparent heat capacity method which includes an additional term for latent heat as shown in Eq. (6)

$$C_P = C_{P,solid}.(1-f_l) + C_{P,liquid}.f_l + \frac{H_m}{\Delta T}f_l \tag{6}$$

where, $C_{p,solid}$ is the heat capacity of the solid phase, $C_{p,liquid}$ is the heat capacity of the liquid phase, H_m is the melting latent heat.

A three-dimensional volumetric heat source with origin (x_0,y_0, z_0) is defined by a Gaussian distribution as given in Eq. (7)

$$Q_{laser}(x,y,z,t) = \alpha\frac{P_l}{\pi r^2 d}e^{\left(-3\frac{\left(x-x_{(t)}\right)^2+\left(y-y_{(t)}\right)^2}{r^2}\right)}e^{\left(-3\frac{\left(z-z_{(t)}\right)^2}{d^2}\right)} \tag{7}$$

where P_l is the power of the heat source, r is the heat source spot radius, d is the thickness of the workpiece, α is the absorption coefficient of material and ($x_{(t)}$, $y_{(t)}$, $z_{(t)}$) is the trajectory of the moving heat source is hence defined by Eq.(8).

$$(x_{(t)},y_{(t)},z_{(t)}) = \begin{cases} (x_0+vt, y_0, z_0) & \text{no oscillation} \\ (x_0+vt-R(1-cos(2\pi ft)), y_0+Rsin(2\pi ft), z_0) & \text{with oscillation} \end{cases} \tag{8}$$

The initial temperature of the workpiece is assumed to be maintained at room temperature (T_0). At the top surface, the heat loss due to convection, radiation and evaporation is governed by Newton's law of cooling and Stefan-Boltzman as follows in Eq. (9). Q_{vap} is the heat loss due to evaporation which is defined as the mass flow rate times the enthalpy of vaporization as defined in [13]. At the bottom surface, heat loss due to vaporization is neglected.

$$-\lambda\nabla T = h(T-T_0) + \varepsilon\sigma\left(T^4 - T_0^4\right) + Q_{vap} \tag{9}$$

The size of the calculation domain is 50 mm × 50 mm × 2 mm and is divided into two plates in butt welding configuration. Tetrahedral mesh is used throughout all computations with very fine

mesh near the weld centerline having a minimum size of 0.1 mm and coarse mesh is used in the rest of the domain. For the heat transfer interface, the direct Parallel Direct Sparse Solver for Clusters (PARDISO) is used and for the fluid flow iterative solver with a relative tolerance of 0.001 is used.

2.3. The relative importance of driving forces on convection from dimensionless numbers

The relative importance of heat transfer by conduction and convection in the weld pool is estimated using the Peclet number, *Pe*, which is defined as [13].

$$Pe = \frac{u\rho C_p L_R}{\lambda} \tag{10}$$

Where u is the characteristic fluid velocity, L_R is the characteristic length taken as the pool radius at the top surface. When $Pe < 1$, the heat transfer in the molten weld pool is primarily by conduction and $Pe > 1$, the primary mechanism of heat transfer is convection. The relative importance of driving forces for fluid flow in the liquid melt pool formed is estimated using the Marangoni number, *Ma*, and the Grashof number, *Gr*. *Gr* is the ratio of buoyancy force to viscous force while *Ma* is the ratio of surface tension gradient force to viscous force. The relative significance of the primary driving forces during fluid flow can be determined by the ratio of these dimensionless numbers as given in Eq. (11) [17]

$$R_{s/b} = \frac{Ma}{Gr} = \frac{L_R\left|\frac{d\gamma}{dT}\right|}{g\rho\beta L_b^3} \tag{11}$$

where L_b is the characteristic length taken as one-eighth of the weld pool radius for buoyancy.

3. Methodology

The commercial COMSOL Multiphysics 5.6 software is used for the numerical simulation of laser welding in butt joint configuration. COMSOL Multiphysics is based on the Finite Element Method (FEM). The calculation domain is discretised into a finite number of elements and general conservation equations are solved on this set of elements. Time is discretised using the backwards differential formula (BDF). The system of non-linear, fully coupled, equations is solved by using the damped Newton method. The heat transfer interface is employed to solve the elliptical partial differential equation in temperature. The three-dimensional model and grid are set using the graphical user interface in the software. A parallel direct solver (PARDISO) is used as it is robust and fast. The domain size, time step and mesh size are investigated to attain high accuracy of the numerical model. The domain size of the numerical model was set large enough to eliminate the boundary effect for fluctuations in the temperature field. The size of the entire simulation domain for a single plate is 50 mm × 25 mm × 2 mm and was divided into three sections with dimensions of 50 mm × 22 mm × 2 mm, 50 mm × 2 mm × 2 mm and 50 mm × 1 mm × 2 mm for better mesh distribution near the weld centreline as shown in Fig. 1. Mesh analysis was performed at a constant material property, welding process parameters and time step. Mesh size is selected which can be solved in reasonable computation time and has less deviation in the global peak temperature. Deviation of temperature is calculated for the maximum temperature over the global domain. Tetragonal mesh is used with a minimum mesh size of 0.1 mm, having a total number of 350,639 mesh elements. The time step is selected based on the frequency of oscillation such that it can map the effect of frequency on the temperature field. Compiled user-defined functions were introduced for the calculation of the position of the heat source at a given time as a function of welding speed, beam oscillation parameters (amplitude and frequency) and the volumetric Gaussian heat source.

4. Results and discussion

4.1. No oscillation condition

The model is validated using the experimental results from the literature [13]. The top surface morphologies of the weld pool and the temperature distribution along the weld centreline have been validated. The length of the melt pool formed is 4.6 mm as shown in Fig. 2 which is comparable to the experimental value of 4.2 mm as measured by using a high-speed camera [13]. The temperature distribution manifests the validity for the heat transfer numerical model and the weld pool morphology manifests the validity for the fluid flow numerical model. Both the weld pool morphology and the temperature profile are in good agreement with the literature.

Table 1 shows the welding process parameters, peak temperature, maximum flow rate, weld dimensions, and the values of dimensionless numbers for both no oscillation and beam oscillation welding. The laser power is kept constant at 4 kW for all cases. For no oscillation welding, peak temperature, width and length of the weld pool and maximum flow rate decrease with an increase in welding speed. This is due to the decrease in the heat input per unit length, described as $(\eta P_l)/V$, which decreases as given in Table 1. With an increase in welding speed, the net heat input to the workpiece decreases and hence peak temperature decreases. But it was found that there is a sharp decrease in length and width of the weld pool as compared to the peak temperature. This shows that the welding speed has more effect on the top surface weld morphologies as compared to the peak temperature. This may be due to the high thermal conductivity of Aluminum where heat is lost quicker at the boundary as compared to the centre. *Pe* is calculated at the rear end of the keyhole in the liquid melt pool and on the weld centreline. It should be noted that *Pe* is a function of position as it depends on u and L_R. It was found that *Pe* decreases with an increase in welding speed which indicates that at lower welding speed convection is more dominant. As welding speed increases, the *Pe* number decreases to a lower value where conduction becomes dominant. This can be attributed to the decrease in the size of the melt pool region formed and the high thermal conductivity of Aluminium. The ratio of Marangoni number to Grashof number $R_{(s/b)}$ increases with the increase in welding speed and is of the order of 10^3-10^4 suggesting that the liquid flow is mainly driven by Marangoni convection due to surface tension force. It was observed that $R_{(s/b)}$ is maximum at the highest welding speed. This signifies that the effect of buoyancy force decreases with an increase in welding speed. The thermal gradient along the fusion zone boundary from the weld centreline increases with an increase in welding speed. This is due to the decrease in the heat input per unit length and the weld width.

4.2. Beam oscillation condition

In beam oscillation welding, the heat source has two kinds of motions, circular motion and linear forward motion in the welding direction. This naturally results in an elliptical motion. The circular part of the motion is governed by the circumferential velocity defined as $2\pi Rf$ and linear forward motion by welding speed S. The net heat input to the workpiece depends on the laser power (P_l) and the welding speed (S) but the heat input per unit length for the beam oscillation welding is defined as $(\eta P_l)/(S + 2\pi Rf)$. Because the actual speed of the oscillating laser beam is much higher than in no oscillation laser welding, the laser beam

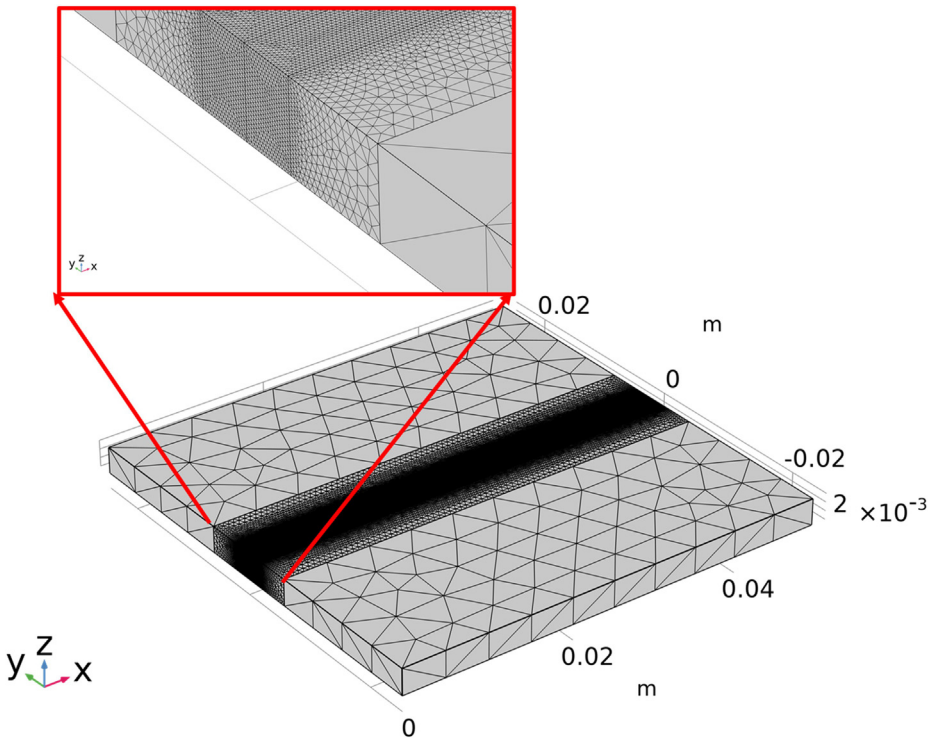

Fig. 1. Schematic illustrations of finite element mesh size and mesh distribution were used for the simulations of a laser welding process.

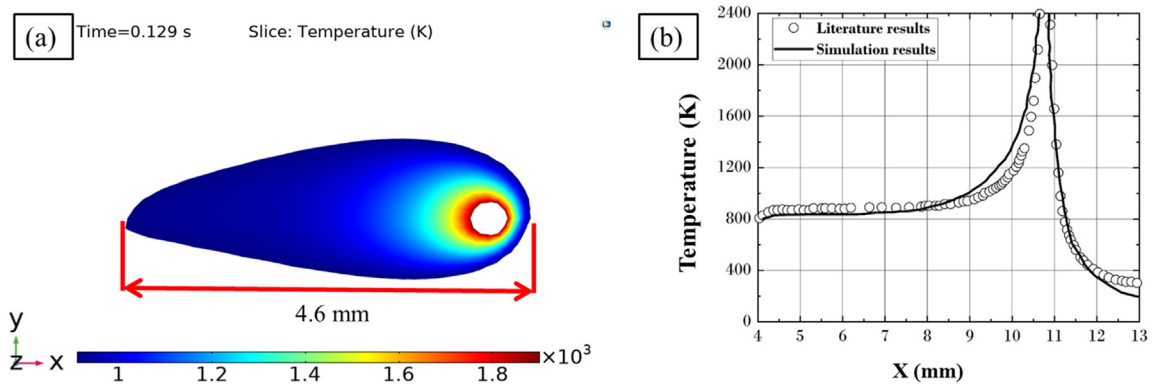

Fig. 2. (a) Weld pool morphologies, simulated from the numerical model. The length of the simulated molten pool is 4.6 mm and 4.2 mm in the experiments [13], (b) Comparison between the calculated and simulated temperature distribution along the weld centreline. Welding parameters are Power (P_l) = 2500 W and welding speed (S) = 80 mm s^{-1}.

Table 1
Welding simulation values of peak temperature (T_{peak}), weld width, length of the weld, maximum flow rate (U_{max}), Peclet number (Pe), the ratio of Marangoni number to Grashof number ($R_{s/b}$), thermal gradient (G) and heat input per unit length.

	S	R	f	T_{peak}	Weld width	Length of weld	U_{max}	Pe	$R_{s/b}$ ($x10^3$)	G	Heat input
	(mm/min)	(mm)	(Hz)	(K)	(mm)	(mm)	(mm/min)			(K/mm)	(J/mm)
No oscillation	1000	–	–	4677	9.9	31.3	1350	3.5	6.4	694	144
	2000	–	–	4194	4.8	14.4	760	0.9	25	869	72
	3000	–	–	3639	3.5	10.1	380	0.3	48	1235	48
Beam oscillation	1000	0.3	600	3882	9.8	27.7	1710	4.3	6.5	506	3.5
	1000	0.6	300	3174	9.7	25.9	1450	3.7	6.2	577	3.5
	1000	0.9	200	2329	9.1	23.3	1110	2.6	7.5	410	3.5

traverses a longer distance in the same amount of time due to additional oscillation. Hence, in the case of beam oscillation, the heat input per unit length is more important to understand while in the case of no oscillation, the total heat input is sufficient to investigate the process. So, the process parameters chosen for beam oscillation welding have an identical heat input per unit length. While comparing beam oscillation with no oscillation welding total heat input is kept constant. Fig. 3 shows the calcu-

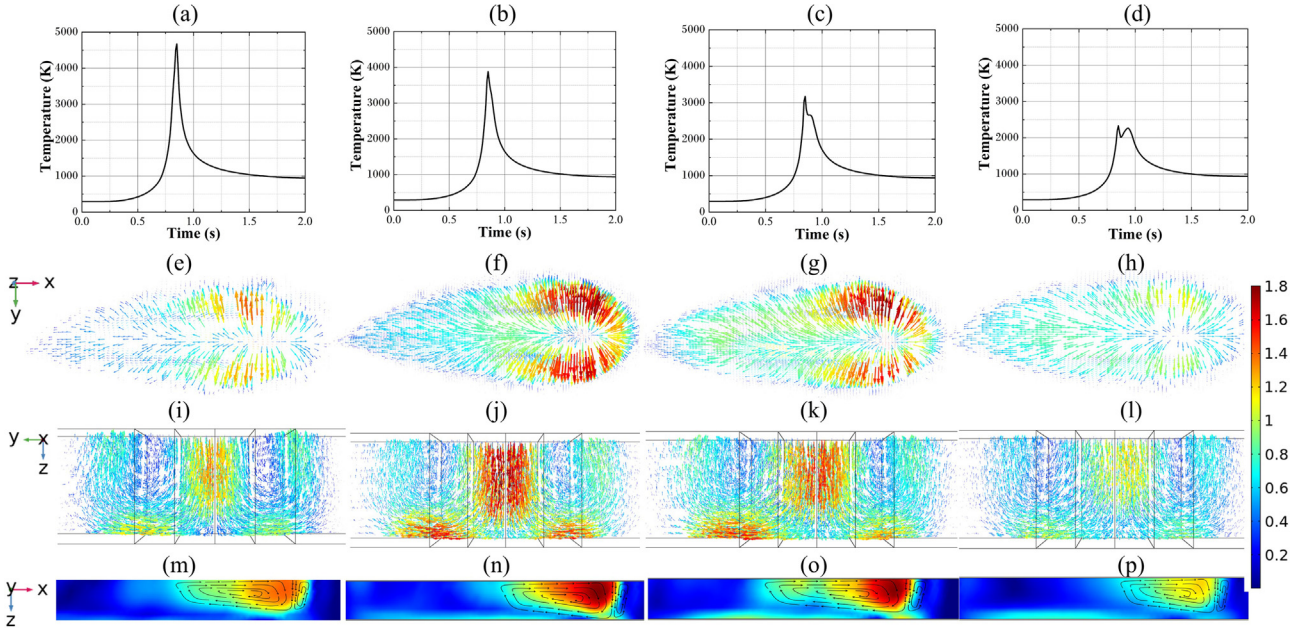

Fig. 3. Calculated temperature (K) variation with time (top row Fig. (a-d)), velocity fields (mm s^{-1}) along *x-y* (top view Fig. (e-h)), *y-z* (front view Fig. (i-l)) and *z-x* (side view Fig. (m-p)) planes for no oscillation welding having (a) P = 4 kW, S = 1 m min^{-1}, and for oscillation welding having constant P = 4 kW, S = 1 m min^{-1}, and varying other parameters as (b) R = 0.3 mm, f = 600 Hz (c) R = 0.6 mm, f = 300 Hz, (d) R = 0.9 mm, f = 200 Hz . For the *x-z* plane magnitude is show using a contour plots and direction of fluid motion using arrows. The flow rate is the absolute velocity magnitude shown is in m min^{-1} scale.

lated weld thermal cycle, weld morphology and velocity fields (along *x-y*, *y-z*, *z-x* planes) for three different cases of beam oscillation whose welding process parameters are given in Table 1. Note that these parameters are selected to have a constant circumferential velocity and constant heat input per unit length. As can be seen from Fig. 3 (e-h), the weld pool is elongated opposite to the welding direction. A typical V-shaped melt contour is formed due to the latent heat of solid–liquid phase transition. The direction and magnitude of the fluid velocity are shown by the length and colour of the arrows. Fig. 3 (e-h) depicts that the flow on the surface points from the centre of the molten pool towards the outward periphery of the molten pool. This is due to the negative temperature coefficient of surface tension $d\gamma/dt$. The force of buoyancy acts in the upward direction. This makes the flow of fluid circulate which can be seen in Fig. 3 (i-l). Also, the flow speed is higher at the top surface of the weld and reduces along the *z*-direction which is shown in Fig. 3 (m-p). The beam oscillation cases are compared with the no oscillation condition, having the same laser power and welding speed such that the total heat input is constant, which is also shown in Fig. 3. The *Pe* number decreases from 4.3 to 3.7 to 2.6 with an increase in *R* while *Pe* for no oscillation condition is 3.5, which shows that convection is again the dominant mode of heat transfer in the weld pool. It is justifiable to use heat transfer and fluid flow model for the analysis of beam oscillation in place of only heat transfer as *Pe* is greater than one. It should be noted that *Pe* changes with the heat input. It increases with the increase in heat input since the maximum velocity increases with an increase in temperature [17]. It is evident from no oscillation conditions, that an increase in welding speed leads to a decrease in the *Pe* number. An increase in welding speed is associated with a decrease in heat input. *Pe* is higher for beam oscillation welding as compared to no oscillation welding for the same welding speed and laser power. This can be attributed to the incorporation of forced convection due to beam oscillation. The ratio of the Marangoni number to Grashof number $R_{(s/b)}$ is of the order of 10^3 confirming that the flow is mainly driven by the surface tension force and to a much lower extent by the buoyancy force. The peak temperature and weld dimensions decrease from no oscillation welding to beam oscillation welding as shown in Fig. 3 (a-d). This is due to the decrease in heat input per unit length. The weld thermal cycle shows a different trend at a higher radius of oscillation. The two peaks in the weld thermal cycle are because the same point gets heated up twice due to a larger oscillation radius for a distance travelled by the heat source in the time between the two peaks in Fig. 3 is equivalent to *2R*. At the longest radius of oscillation, the peak temperature is below the boiling point which suggests that there is no formation of a keyhole. During beam oscillation welding, the peak flow rate decreases with an increase in the radius of oscillation (values given in Table 1). This can be attributed to the decrease in the frequency of oscillation which leads to a decrease in the forced convection due to beam oscillation. With the increase in radius of oscillation, the high-speed flow area gradually increases as shown in Fig. 3. The thermal gradient along the fusion zone from the weld centreline decreases from no oscillation welding to beam oscillation welding due to repeated heating and melting.

5. Conclusions

Numerical studies between no oscillation welding and oscillation welding, using the same total heat input, were carried out. The Peclet number was used to describe the ratio between heat transport by convection and conduction. In the case of no oscillation welding, the Peclet number decreases as the welding speed increases which indicates that the heat transfer is dominated by conduction rather than convection. In the case of beam oscillation welding, a constant circumferential velocity was maintained for all cases in this study. Here, the Peclet number decreases as the radius of oscillation are increased whilst the heat transfer remained to be dominated by convection. Comparing no oscillation welding with beam oscillation welding shows that the Peclet number for no oscillation is greater than the value for the largest radius of oscillation. In combination with the flow profiles for larger radii,

which become similar to no oscillation welding conditions, it can be inferred that the change in Peclet number is attributed to differences in thermal conduction of the oscillating heat source. This could potentially serve as a critical limit for the oscillation radius where both welding conditions are indeed similar in terms of heat transport. Furthermore, the ratio of the Marangoni number to the Grashof number is of the order of 10^3, suggesting that surface tension force is dominant rather than buoyancy force in all cases. Given a constant circumferential velocity in all oscillating welding conditions, it was found that peak temperature, weld dimensions and the thermal gradient decrease with an increase in oscillation radius. At the same time, the peak flow rates in the melt pool, however, decrease. It can therefore be concluded that beam oscillation offers two additional parameters to control fluid flow and heat transport to optimise welding performance.

CRediT authorship contribution statement

Anand Mohan: Conceptualization, Methodology, Software, Validation, Formal analysis, Investigation, Visualization, Writing – original draft. **Dariusz Ceglarek:** Supervision. **Michael Auinger:** Supervision, Writing – review & editing.

Declaration of Competing Interest

The authors declare that they have no known competing financial interests or personal relationships that could have appeared to influence the work reported in this paper.

Acknowledgements

This work is supported by the WMG, University of Warwick (United Kingdom), and the Indian Institute of Technology Kharagpur (India) as the financial support for the PhD studentship via the WMG-IIT partnership program.

References

[1] D. Ceglarek, M. Colledani, J. Váncza, D.Y. Kim, C. Marine, M. Kogel-Hollacher, A. Mistry, L. Bolognese, CIRP Ann. - Manuf. Technol. 64 (2015) 389–394.
[2] T. Sun, P. Franciosa, M. Sokolov, D. Ceglarek, Procedia CIRP 94 (2020) 565–570.
[3] S.K. Dinda, D. Das, A. Mohan, P. Srirangam, G.G. Roy, Metall. Mater. Trans. A (2021) 1723–1731.
[4] G.M. Reddy, C.V.S. Murthy, N. Viswanathan, K.P. Rao, Sci. Technol. Weld. Join. 12 (2007) 106–114.
[5] C. Thiel, A. Hess, R. Weber, T. Graf, in: Laser Sources Appl., SPIE, 2012, p. 84330V.
[6] F. Hugger, K. Hofmann, S. Kohl, M. Dobler, M. Schmidt, Weld. World 59 (2015) 165–172.
[7] K. Hao, G. Li, M. Gao, X. Zeng, J. Mater. Process. Technol. 225 (2015) 77–83.
[8] Z. Wang, J.P. Oliveira, Z. Zeng, X. Bu, B. Peng, X. Shao, Opt. Laser Technol. 111 (2019) 58–65.
[9] F. Fetzer, M. Sommer, R. Weber, J.P. Weberpals, T. Graf, Opt. Lasers Eng. 108 (2018) 68–77.
[10] L. Wang, M. Gao, C. Zhang, X. Zeng, Mater. Des. 108 (2016) 707–717.
[11] K. Rubben, H. Mohrbacher, E. Leirman, Lasers Mater. Process. 3097 (1997) 228–241.
[12] K. Abderrazak, S. Bannour, H. Mhiri, G. Lepalec, M. Autric, Comput. Mater. Sci. 44 (2009) 858–866.
[13] S. Geng, P. Jiang, X. Shao, L. Guo, X. Gao, J. Mater. Sci. Technol. 46 (2020) 50–63.
[14] T.M.P.L. Busuttil, Laser Welding Apparatus and Method for High Temperature Gradient Cooling Alloys, Patent Number-5665255 (1997).
[15] A. Mohan, D. Ceglarek, M. Auinger, Int. J. Adv. Manuf. Technol. 121 (2022).
[16] C.S. Wu, T. Zhang, Y.H. Feng, Int. J. Heat Fluid Flow 40 (2013) 186–197.
[17] X. He, J.W. Elmer, T. Debroy, J. Appl. Phys. 97 (2005) 084909.